Coherent behavior of balls in a vibrated box

Yves Garrabos, Pierre Evesque, Fabien Palencia, Carole Lecoutre-Chabot, Daniel Beysens

Coherent behavior of balls in a vibrated box

Y. Garrabos[(1)], P. Evesque[(2)], F. Palencia[(1)], C. Lecoutre[(1)], and D. Beysens[(3)]
[(1)] *ESEME-CNRS, ICMCB-UPR 9048, Université Bordeaux I, 87 avenue du Docteur Albert Schweitzer, F-33608 Pessac France;*
[(2)] *LMSSMat-CNRS-UMR 8579, Ecole Centrale Paris, F-92295 Châteney-Malabry France; and*
[(3)] *ESEME-CEA, SBT, CEA-Grenoble, F-38054 Grenoble Cedex 9, France.*
(Dated: revised 28 July, 2004)

We report observations on very low density limit of one and two balls, vibrated in a box, showing a coherent behavior along a direction parallel to the vibration. This ball behavior causes a significant reduction of the phase space dimension of this billiard-like system. We believe this is because the lowest dissipation process along a non-ergodic orbit eliminates ball rotation and freezes transverse velocity fluctuations. ¿From a two-ball experiment performed under low-gravity conditions, we introduce a "laser-like" ball system as a prototype of a new dynamical model for very low density granular matter at nonequilibrium steady state.

PACS numbers: 05.45.-a, 45.50.-j, 45.70.-n, 81.70.Bt, 81.70.Ha, 83.10.Pp

The present letter starts with the experimental study of the dynamical behavior of a single ball vibrated in a three-dimensional (3D) box. It can be viewed as a 3D experimental version of accelerator models of particle physics impacting oscillating heavy objects, and vibrating billiard type systems, where the physics of ergodicity, i.e., filling of the available phase space by stochastic motion, can be examined from the bouncing ball models [1, 2, 3]. Figs. 1a and 1b give schematic presentation of the two most known accelerator models of one bouncing ball, the so-called Pustylnikov and Ulam versions of the Fermi acceleration mechanism (see [1] and references therein for details). In the Pustylnikov version, the ball moves freely above the vibrating wall, under a constant acceleration (here the g_0 Earth's gravity acceleration), while in the Ulam version, the particle moves with constant velocity between impacts with two walls - one vibrating and one fixed.

It can be studied also as the ultimate limit for a forced dilute granular gas [4], when grain-grain collisions are negligible. This can occur, for example, in a cubic cell when the small amount N of grains only covers a very small fraction of one vibrating wall surface. Therefore, the grain mean free path l_g between two grain-grain collisions is much larger than the cell size L, corresponding to the so-called Knudsen-like regime [5]. Most of the grains are in a ballistic motion between one vibrating wall and the lid, or between two vibrated walls, following the selected experimental configuration of the container. Thus, the low density limit of a non-interacting granular matter is reached after a progressive reduction of the dissipated internal energy. This reduction is due to the decreasing frequency of the inelastic grain-grain collisions.

Our basic understanding of single particle dynamics comes from $1\,g_0$ experiments of one bouncing ball (diameter ϕ) on a vibrating plate, when the restitution coefficient ε associated with the ball-plate contact exhibits a finite value $0 < \varepsilon \leq 1$ [6, 7, 8]. The analysis of the results is mainly concentrated on the rich phase space for the long-term behavior of this impacting system, which makes questionable the experimental conditions to observe the evolution to chaos [6]. Thus, our initial intuition suggests that the ball dynamics in a finite-sized box remains poorly affected by a second wall, provided that the wall-plate distance L is larger than the vibration amplitude A_p. In fact, as demonstrated in $1\,g_0$ and random-*low* (< 1) g_0 experiments below, the assumption where stochastic trajectories of the ball occur as the most probable dissipative situations for the long-term behavior of the system, is not realistic *within a large plate velocity range*. On the contrary, the ball tends to behave quasi-instantaneously as a regular particle in a 1D vibrating cavity with the translation motion parallel to the vibration direction. In the same time, a significantly audible sound is generated by the characteristic resonant "impact noise". The ball resonant behavior demonstrates a drastic reduction of the phase space dimension because

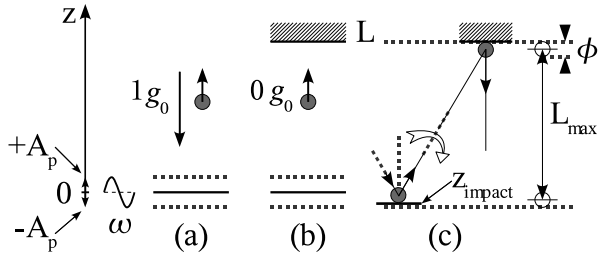

Figure 1: (a) Pustylnikov version of the Fermi acceleration, in which a ball returns to an oscillatory wall under the g_0 Earth's gravity acceleration (see [1, 3] and references therein); (b) Ulam version, in which a ball bounces back and forth between an oscillating wall and a fixed wall separated by distance L under $0\,g_0$ (see [1, 2] and references therein); (c) schematic illustration of the ball rotation and transverse velocity fluctuations frozen in the dissipative Ulam version with restitution coefficient $\varepsilon < 1$. The particle motion appears then quasi-1D and regular, with a significant increase of its average energy due to a non-stochastic acceleration when the wall oscillation is a periodic function of time.

the second wall increases the dissipation, eliminating the rotation of the ball and freezing its transverse velocity-fluctuations after a very few number of back and forth, as schematically shown on Fig. 1c and as discussed below. The gain on the mean velocity of the resonant ball is used here to report very accurate variations of the normal restitution coefficient as a function of the ball velocity.

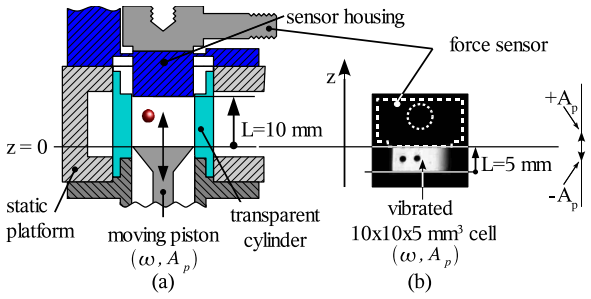

Figure 2: (a) Experimental set-up of the Ulam model for 1-ball ($\phi = 2.0\,mm$ diameter), used for ground-based studies (z-axis parallel to Earth's gravity direction) and for low-gravity studies (residual random acceleration $\leq 5\,10^{-2}\,g_0$) during parabolic flights of the CNES-A300-ZeroG airplane. (b) Part of video picture showing 2-ball coherent flight positions ($\phi = 1.2\,mm$ ball diameter), vibrated along the z-axis at $f = \frac{\omega}{2\pi} = 14.75\,Hz$ and $A_p = 0.3241\,mm$, in very low-gravity conditions (residual random acceleration $\leq 10^{-4}\,g_0$), during our experiment on the ESA-funded sounding rocket Maxus 5 (see text). The sensor location appears in dashed line.

Our first experiment studies the dynamics of a single ball in a static cylindrical cell of $L = 10\,mm$ height, closed at the bottom by a vibrating piston (Fig. 2a). The piston moves along the z-axis, according to $z = A_p sin\,[\omega t]$ (i.e. acceleration $g_z = -\Gamma_p sin\,[\omega t]$ with $\Gamma_p = \omega^2 A_p$). g_z-accelerations are monitored using a piezoelectric tri-axial accelerometer (PCB Piezotronics, Model M356A08) attached to the moving part of an electromagnetic shaker. The piston, $D_p = 12.7\,mm$ in diameter, is made from type AISI 316L stainless steel. The static transparent cylinder, $13.0\,mm$ inner diameter, $20\,mm$ outer diameter, and $22\,mm$ height, is made from PMMA. At the top of the cell, the ball impacts the flat cylindrical cap (12.7 mm diameter, 9.0 mm thickness) of a covered-sensor housing made from type 17-4 stainless steel, in contact with the flat sensing surface of a force sensor (PCB Piezotronics, Model 200B02). The ball resonant motion is observed by stroboscopic illumination at the shaker frequency. The signals from the z-axis accelerometer and the force sensor are recorded with a resolution of $0.5\,\mu s$. Amplitude, frequency, and acceleration ranges used here are $0.44\,mm < A_p < 0.62\,mm$, $30\,Hz \lesssim f = \frac{\omega}{2\pi} \lesssim 120\,Hz$, and $3\,g_0 < |g_z| < 40\,g_0$, respectively.

This vibrating facility was operated both on ground and under reduced-gravity conditions, during parabolic flights on the French Space Agency (CNES) A300 ZeroG airplane. One experimental run time covers a typical Δt duration of $\simeq 20\,s$, (the low-gravity period of a parabolic flight), during which the numerical data are stored.

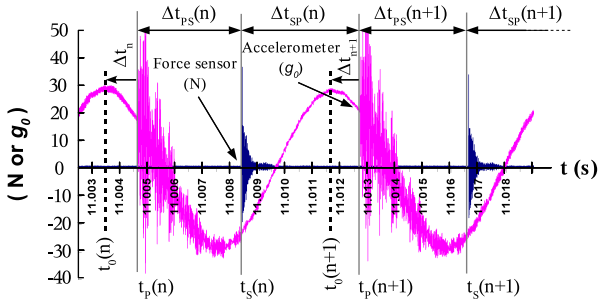

Figure 3: $1\,g_0$ synchronized signals of the z-axis accelerometer and force sensor showing impact times (lower) and flight times (upper) for back and forth resonant behavior of a single ball at $f = 121.2\,Hz$ with $A_p = 0.486\,mm$. For each period, $t_0\,(n)$ corresponds to the piston position $z\,[t_0\,(n)] = -A_p$, where the length cavity is maximum (see text).

Fig. 3 reports typical signals for a ball resonant behavior in the case of one stainless steel spherical ball, $\phi = 2.000 \pm 0.002\,mm$ in diameter, vibrated at $f = 121.2\,Hz$ with $A_p = 0.486\,mm$ ($\Gamma_p = 28.7\,g_0$). The z-axis accelerometer response to each ball-piston impact is superimposed on the sinusoidal variation of g_z-component. This figure gives a typical sequence of n, $n+1$ resonant impacts on the piston (subscript P) and on the force sensor cap (subscript S). The reference time $t_0(n) = \frac{3n}{4f}$ of the n^{th} sequence starts at the time when the piston reaches its maximum amplitude position for which the cavity length is maximum. $\Delta t_n = t_0\,(n) - t_P\,(n)$ is the time delay for the n^{th} ball-piston impact at $t_P\,(n)$, where the piston position is $z_{impact}\,(n) = -A_p cos\,[\varphi_n]$, associated to the impact phase $\varphi_n = -2\pi f \Delta t_n$. The impact times, $t_P\,(n)$, $t_S\,(n)$, the flight times, $\Delta t_{PS}\,(n)$, $\Delta t_{SP}\,(n)$, the time delay Δt_n, the impact position $z_{impact}\,(n)$ and phase φ_n of the piston, are then obtained by numerical data analysis over each run time Δt. Our measurement precision ($\leq 5\,\mu s$) of relative times appears to be much bigger than in previous bouncing ball experiments [9, 10].

The ideal resonant behavior over Δt, gives $n_{T,ideal} = f\Delta t$ for the ideal total impact number, while our statistical signal analysis counts the effective impact number $n_{T,eff}$. Fig. 4a gives the ball resonance rate (%), $\left(\frac{n_{T,eff}}{n_{T,ideal}} \times 100\right)$, as a function of f, for a nearly constant amplitude value $A_p \simeq 0.5\,mm \simeq \frac{L}{20} \simeq \frac{\phi}{4}$. The results from $1\,g_0$ (full diamonds) and $\leq 5\,10^{-2}\,g_0$ (open diamonds) experiments are reported. Fig. 4a shows that the ball resonant behavior is all the more frequent as f increases and gravity level decreases. This result enhances the relative influence of the gravity effects and/or of the finite size effects at low frequency.

In addition, the φ_n statistical analysis provides the $\frac{\langle |z_{impact}| \rangle}{A_p} = cos\,[\langle \varphi \rangle]$ behavior as a function of f which is reported on Fig. 4b ($\langle x \rangle$ corresponds to x mean value).

The resonance corresponds to the nearly-maximal length of the cavity for which the gain on the ball energy is then a (maximal) extremum, while the wall velocity at the impact tends to a (minimal) extremum (close to zero). These results can be understood in terms of the small but finite impact dissipation of energy ($\sim 1-\varepsilon^2$), with $\varepsilon < 1$. The periodic condition at $0\,g_0$ gives $v_{b,up} = \frac{1+\varepsilon_P}{1-\varepsilon_P\varepsilon_S} v_p$ and $v_{b,down} = -\frac{(1+\varepsilon_P)\varepsilon_S}{1-\varepsilon_P\varepsilon_S} v_p$, where v_p, $v_{b,up}$, and $v_{b,down}$, are the respective velocities for the piston, for the ball moving up from the piston to the sensor cap, and down from the sensor cap to the piston. ε_P and ε_S are the respective restitution coefficients for the ball-piston and ball-sensor cap contacts. The regular behavior at fixed values of $L-\phi$, ε_P, ε_S, f and A_p, satisfies

$$\alpha + cos\,[\langle\varphi\rangle] = \beta sin\,[\langle\varphi\rangle] \qquad (1)$$

with $\alpha = \frac{L-\phi}{A_p}$ and $\beta = 2\pi\frac{1+\varepsilon_P}{1+\varepsilon_S}\frac{\varepsilon_S}{1-\varepsilon_P\varepsilon_S}$. This non-equilibrium steady state expresses the balance between forced and dissipated energies, which occurs for one single mean reduced length of the cell (given by the left hand member of Eq. (1)). That corresponds to a single mean momentum exchange in the simplified Ulam version [1, 2, 3] for $\varepsilon < 1$, in which the moving wall imparts momentum to the ball but occupies a fixed position.

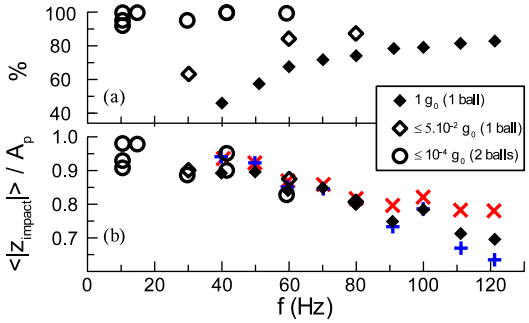

Figure 4: (a) Ball resonance rate (%); (b) Relative wall position at the ball impact time. Full diamonds) 1-ball $1\,g_0$ experiment; Open diamonds) 1-ball airplane experiment; Open circles) 2-ball Maxus-5 experiment. In (b), black + and grey × correspond to the $cos\,[\langle\varphi\rangle]$, with the $\langle\varphi\rangle$-determination from Eq. (1), for $\langle\varepsilon_S\rangle = \langle\varepsilon_P\rangle = \varepsilon$ mean values shown in Fig. 5, at each selected $\{f; A_p\}$ run (note the agreement with direct analysis of $\frac{\langle|z_{impact}|\rangle}{A_p}$). $|z_{impact}|$ corresponds to the position of the flat top of the piston (1-ball experiment), or the flat cap of the force sensor (2-ball Maxus-5 experiment).

Therefore, our accurate velocity measurements associated with the regular behavior of the ball provide direct access to $\varepsilon_S = -\frac{v_{b,down}}{v_{b,up}}$ and $\varepsilon_P = \frac{v_{b,up}-v_p}{v_p-v_{b,down}}$. Fig. 5 shows the statistical behavior of ε_S (black +), and ε_P (grey ×), as a function of $v_i = v_{b,down}$, and $v_i = v_{b,up}$, respectively (accounting for gravity effects). We observe that $\varepsilon_P \cong \varepsilon_S$, leading to simplified forms of above relations. That permits to check the validity of the Eq.(1), as shown by $cos\,[\langle\varphi\rangle]$ values (black + and grey ×), reported in Fig. 4b, which have been obtained using $\langle\varepsilon_S\rangle = \langle\varepsilon_P\rangle = \varepsilon$ mean values, (black + and grey ×, within white square), shown in Fig. 5, for each selected $\{f, A_p\}$ pair. We also note that our ε measurements are in sharp contrast with the solid curve representing a recent fit of former results [11] (see also Ref.[12]). It highlights that only the absence of significative ball rotation can explain such ε high values.

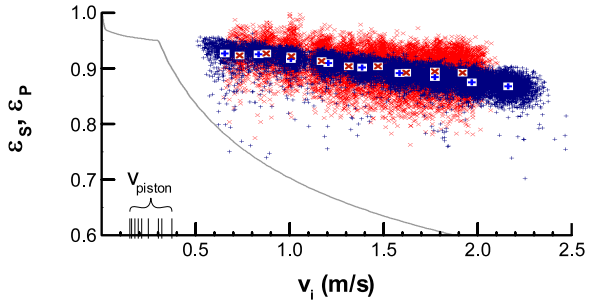

Figure 5: ε_S (black +), and ε_P (grey ×), measurements for ball-sensor cap and ball-piston contacts (see text), according to ball incident velocity ($1\,g_0$ experiments). Symbols in white squares correspond to associated mean values which are used for$\langle\varphi\rangle$-determination from Eq. (1), for each selected $\{f; A_p\}$ run (see Fig. 4b). The maximum velocity range for our vibrating piston is indicated on the v_i-axis below the bracket. The full curve corresponds to a fit [11] of previous measurements. The decrease in restitution at large velocity is interpreted as being due to plasticity effects in the solid [12].

A second experiment was performed on the Maxus-5 sounding rocket funded by the European Space Agency (ESA), where residual random acceleration was $\leq 10^{-4}\,g_0$. For the first time, this experiment studies the dynamics of two hard-brass spherical balls, $\phi = 1.190 \pm 0.002\,mm$ in diameter, in a vibrating parallelepipedic box of $5\,mm$ height and $10\times10\,mm^2$ internal cross section, where the sensitive cap of the force sensor is used as an opposite cell-wall (see Fig. 2b for details). The experimental conditions maintain the ratio relation $\frac{A_p}{L} \simeq \frac{1}{4}\frac{\phi}{L}$. Fig. 6a is similar to Fig. 3, except that the sensor position and the ball-sensor impact force are the only recorded signals. Fig. 6a evidences nearly ideal concomitancy of the 2-ball resonant behaviors during a time period of $500\,ms$ selected among the $65\,s$ run at $f = 14.75\,Hz$, with $A_p = 0.3241\,mm$ ($\Gamma_p = 0.3\,g_0$). The $\Delta t_n = t_0\,(n) - \frac{1}{2}\left[t_{S,1}\,(n) + t_{S,2}\,(n)\right]$ values for the n^{th} 2-ball impacts occurring at $t_{S,1}$ and $t_{S,2}$, respectively, are reported on Fig. 6b, for a total number of recorded impacts ($2n_{T,eff} = 1906$) very close to ideal value ($2n_{T,ideal} = 1918$). This figure illustrates the quasi-perfect coherent behaviors of the two balls during this long run time. This coherent behavior is called hereafter the "laser-like" behavior for granular matter at very low density. Fig. 4a (open circles) shows that this "laser-like" behavior approaches the 100% ball resonance rate in weightlessness for a significative range of low frequencies, confirming then the gravity-sensitivity of the ball

acceleration mechanism. Fig. 4b (open circles) extends the behavior of the (sensor) wall mean position at impact times to the low frequency range.

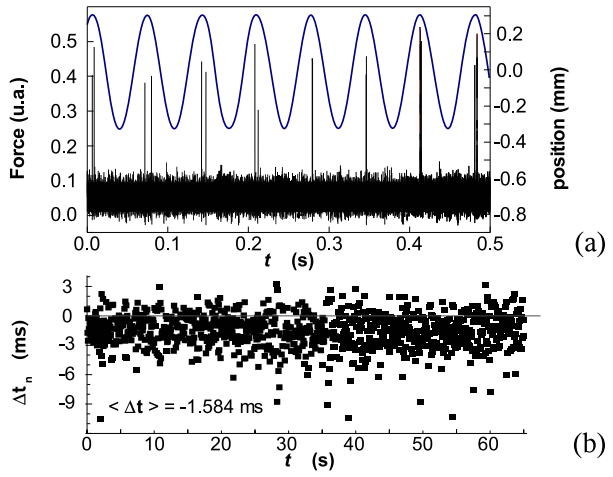

Figure 6: (a) low-gravity typical resonant behavior of two balls (ESA Sounding rocket Maxus-5 experiment) for a period of $500\,ms$ selected among a vibration run at $f = 14.75\,Hz$ with $A_p = 0.3241\,mm$ amplitude; upper) z-position of the vibrated box ; lower) force sensor response showing regular two ball impacts; (b) Variation of $\Delta t_{n,}$ (mod f^{-1}) along the $65\,s$ of the run, corresponding to $2n_{T,eff} = 1906$ impacts of the 2 balls during their "laser-like" behavior (see text). Time reference is when position is maximum (see Fig. 2b and text). The mean value is $\langle \triangle t \rangle = (n_{T,eff})^{-1} \sum_n \Delta t_{n,}$.

We can approach the inelastic ball resonant behavior from a billiard-like viewpoint where closed orbits are not ergodic, i.e. the so-called eigen modes of the billiard cavity. The vibration excites the ball motion on these modes. Those that dissipate too much cannot be sustained, while those that dissipate too little do not exist or split precisely on eigen modes. Therefore, in our present 3D-configuration of the box, only a few eigen modes can be excited by vibrations. That explains the few possible orbits (such as the observed one, parallel to the vibration direction) which act as attractive basins with lowest dissipation. Thanks to this phenomenon, the real shape of the cavity should play a role in the ergodic/non-ergodic problem. However the ball orbit parallel to the vibration direction remains stable, for example when we tilt (up to 10°) the sensor cap surface compared to the perpendicular direction of the vibration (which simulates a distorsion of the cavity shape), or when we add a second ball of lower diameter (which simulates an obstacle within the cavity). That confirms the loss of ergodicity in this 3D experimental problem and the reduction of the non-interacting-ball phase space by dissipation. Each 1-ball phase space typically goes from a 11D space (3D for positions, 2D for rotations, 5D for associated velocities, and 1D for time) to a 1D space (for time).

Considering the fact that this observed resonant behavior cannot correspond to the case of the so-called Knudsen-like regime ($l_g \gg L$), in which particles explore space ergodically but do not increase their energy on the average, we conclude that our understanding of the very low density limit of a non-interacting granular matter should be revisited, in the absence of gravity, in order to investigate : i) the "low-energy" regime, corresponding to small aspect ratio $\frac{v_{piston}}{v_{ball}} \approx \frac{A_p}{L-\phi} \ll 1$, which can permit one to check the relevance of a threshold value $\left(\frac{v_{piston}}{v_{ball}}\right)_{th} \lesssim 1-\varepsilon$ needed to observe some more irregular motion; ii) the "high-energy" regime, corresponding to larger values of the surface ratio $N\left(\frac{\phi}{D_p}\right)^2$, for which we can expect that above a possible threshold number N_{min} of balls (which remains to be determined), the presently observed "laser-like" behavior could be replaced by the classical dynamical behavior where more frequent inelastic interparticle collisions increase dissipation and restore the ergodic motion of a dilute granular "gas".

We thank S. Fauve and E. Falcon for helpful discussions. This work was supported by CNES and ESA. The authors gratefully acknowledge Novespace and "Centre d'Essais en Vol" teams for their assistance during A300 Zero-G airplane experiments. The TEM-FER Maxus 5 experimental module has been constructed by EADS Space Transportation (Germany). We gratefully acknowledge the Maxus team for its technical assistance.

[1] A. J. Lichtenberg, M. A. Lieberman and R. H. Cohen, Physica D **1**, 291 (1980).
[2] P. J. Holmes, J. Sound and Vibration **84**, 173 (1982).
[3] A. J. Lichtenberg and M. A. Lieberman, *Regular and Chaotic Dynamics*, Applied Mathematical Sciences Vol. 38 (Springer-Verlag, New York, 1992) .
[4] J. S. Olafsen and J.S. Urbach, Phys. Rev. Lett **81**, 4369 (1998) ; Phys. Rev. E **60**, R2468 (1999).
[5] P. Evesque, D. Beysens, and Y. Garrabos, J. Phys. IV France **11**, Pr6-49 (2001).
[6] J. M. Luck and A. Mehta, Phys. Rev. E **48,** 3988 (1993).
[7] S. Warr, W. Cooke, R. C. Ball, J. M. Huntley, Physica A **231**, 551 (1996), and references therein.
[8] J.-C. Géminard and C. Laroche, Phys. Rev. E **68**, 031305 (2003).
[9] L. Labous, A. D. Rosato, and R. N. Dave, Phys. Rev. E **56**, 5717 (1997).
[10] I. Stensgaard and E. Lægsgaard, Am. J. Phys. **69**, 301 (2001).
[11] S. McNamara, E. Falcon, in *Granular Gas Dynamics*, Lecture Notes in Physics **624**, T. Pöschel and N. V. Brilliantov Eds. (Springer-Verlag, Berlin, 2003) p. 347.
[12] W. Goldsmith, *Impact : The theory and physical behavior of colliding solids* (Edward Arnold Pubs. LTD, 1960).